The effect of leading edge porosity on airfoil turbulence interaction noise

Luke Bowen,[1, a)] Alper Celik,[2] Beckett Zhou,[1] Michelle Fernandino Westin,[3] and Mahdi Azarpeyvand[1]

[1] *Faculty of Engineering, University of Bristol, Bristol, BS8 1TR, United Kingdom*

[2] *Aerospace Engineering, Swansea University, Swansea SA1 8EN, United Kingdom*

[3] *Embraer S.A., São José Dos Campos, SP 12227-901, Brazil*

(Dated: 12 October 2022)

Airfoil-turbulence interaction noise and the flow-field up to and over the porous leading edge is experimentally studied. The porous leading edges were of the same base Triply Periodic Minimal Surface structure with varying porosity to understand how the porosity, permeability and pore size affect the generated turbulence interaction noise. The turbulent flow was generated by the means of a passive turbulence grid which does not affect the normal background noise of the wind tunnel. Far-field noise results were obtained from a polar microphone array to assess the directivity of the sound as well as the narrowband frequency contributions. Far-field noise results demonstrate that increasing porosity reduces the turbulence interaction noise over low-to-mid frequencies, with a penalty of a high-frequency noise increase. Flow measurement results indicate hydrodynamic penetration of the flow into the porous structure at the leading edge. Furthermore, the two-point correlation analysis of the velocity fluctuations approaching the leading edge, show that the turbulent structures approaching the solid leading edge appear to deform into more two-dimensional structures. Whereas, in the case of the porous leading edge the turbulent structures appear to retain a strong spanwise coherence up to the point of hydrodynamic penetration.

[a]luke.bowen@bristol.ac.uk

I. INTRODUCTION

As noise becomes an ever-increasing environmental concern, turbulence interaction noise is an important phenomenon to be addressed in the drive towards quieter propulsion. Highly rotational, turbulent flows generated by fan blades interact with stator vanes for the purpose of flow straightening. Turbulent structures in the wake of the fan, interact with the leading edge of the stator and subsequent pressure fluctuations on the surface of the airfoil generate noise. The efficiency of noise generation in airfoil turbulence interaction is dictated by the ratio of the size of the turbulent structures, to the leading edge radius of the airfoil.

Turbulence interaction noise is a subject that has been of large social interest since the fundamental study by Amiet[1]. Amiet proposed a model[1] which can predict the interaction noise by implementing linearized airfoil theory to calculate the aerodynamic response of the incident gust on the airfoil; then calculating the unsteady lift propagation to the acoustic far-field accounting for scattering and mean flow effects. Paterson and Amiet[2] showed turbulence impingement as low frequency dominating noise radiation, considering the scale of turbulence is large. Angle of attack effects were studied by Moreau and Roger[3] showing that for noise generation in turbulent flow there is almost no dependency to angle of attack. More commercial type airfoils were studied by Devenport *et al.*[4], where thickness and camber effects of real airfoils were studied for a turbulent flow. Devenport *et al.*[4] concluded that although angle of attack has a strong effect on the airfoil response function, it only has a small effect on noise generation. Varying the turbulent flow has been shown to be just as important as varying the airfoil and this was extensively studied by Hutcheson *et al.*[5].

Their tests consisting of a host of different inflow conditions and geometries, finding that as length scale and intensity increased this uniformly increased the spectral levels. Both airfoil geometry and the turbulent inflow are important factors in the noise generation and there have been a host of research on the topic[3,4,6–8], all concluding that the airfoil geometry does in fact alter the noise generation in turbulent flow.

Passive noise control techniques have shown to be effective in airfoil noise reduction when implemented to trailing edge configurations[9–15]. Further works have showed the potential of porous materials for noise reduction[9,16–19], but a common conclusion is found that better understanding of the mechanisms and flow interaction is needed to optimize the implementation of porous materials for the noise abatement. As with previous studies[9,10] they found that the porous material will decrease the low frequency noise contribution and increase it at high frequency, suggesting the influence due to surface roughness[20]. Furthermore, turbulence interaction noise has been shown to be reduced by using passive leading edge treatments and in recent years serrated leading edge configurations have gathered much interest[21–25].

The reduction of turbulence interaction noise with the use of a porous leading edge has been the subject of much interest[17,26–30]. Sarradj and Geyer were the first to rekindle the interest in porous airfoils and carried out the first study on the effect of a fully porous airfoil[29]. The study focused on changing porous properties of airfoils to assess the acoustic benefit, a reduction in noise in most cases was found at the detriment to the overall hydrodynamic performance of the airfoil. Geyer *et al.*[27] studied leading edge noise reduction using fully porous airfoils finding that a reduction in air flow resistivity increases the noise reduction. Geyer *et al.*[16] further developed the porous leading edge idea by adding perforations at the leading edge of the airfoil, with the remaining chord of the airfoil solid. A noise reduction of up to 8dB was observed and a reduction in the aerodynamic loses compared to the fully porous airfoils. Roger and Moreau[31] used grid generated turbulence to measure the effect that a steel-wool filled NACA 0012 had on noise radiation and showed a maximum of 5dB of noise reduction is achievable from a suboptimal approach. Sinnige *et al.*[19] studied the effect of a flow-permeable perforated leading edge for the reduction of the noise generated on a pylon in the slip-stream of a propeller, in which a measured reduction of the far-field tonal noise was observed. A further step in the characterization of leading edge noise reduction was achieved by Zamponi *et al.*[32] who studied the effect of a porous airfoil on the rapid-distortion of turbulent structures near the leading edge. This experimental and numerical study indicated a reduction in the upwash component of the root-mean-square (rms) of the velocity fluctuation as one of the contributing factors to the reduction of the far-field noise. Chaitanya *et al.*[33] experimentally demonstrated that perforations downstream of the leading edge of a flat plate can reduce the turbulence interaction noise, and used a simple analytic model to show the reduction of noise spectra collapses when plotted against non-demensional frequency. Ocker *et al.*[34,35] demonstrated the noise reduction of a partially porous fan blade, and showed that preserving the solid structure at the leading edge, follow by a porous section immediately downstream can improve both the aerodynamic and aeroacoustic performance. This paper seeks to assess the reduction of airfoil-turbulence interaction noise with porous leading edges of varying porosity. Furthermore, the study considers how the flow approaching and over the leading edge is affected by the introduction of the porous leading edge to offer insight to the noise reduction. The paper is organized as follows: Section II describes the

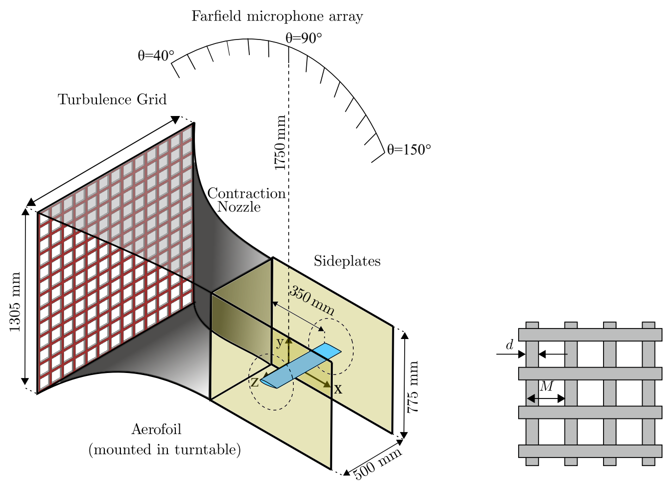

FIG. 1. Schematic of airfoil set-up with turbulence grid and far-field array in the Aeroacoustic Wind tunnel.

wind tunnel, measurement set up porous structure and airfoil. Section III presents the results and discussions of the far-field noise and the velocity field analysis and Section IV concludes this manuscript.

II. MEASUREMENT SETUP

A. Wind tunnel and model

The airfoil turbulence interaction noise experiments were performed in the University of Bristol Aeroacoustic Facility, which is a closed-circuit, open-jet anechoic wind tunnel. The chamber has physical dimensions of 6.7 m × 4.0 m × 3.3 m and is anechoic down to 160 Hz[36]. Figure 1 displays a schematic of the wind tunnel contraction with the turbulence grid mounted in the contraction nozzle and the airfoil mounted within sideplates, 350 mm downstream of the contraction nozzle outlet. The contraction nozzle outlet has physical dimensions of 500 mm in width and 775 mm in height, which allows for a steady operation from 5 m/s to 45 m/s and a normal turbulence intensity level below 0.2%[36].

This study was conducted with a NACA 0012 profile airfoil that features an interchangeable leading edge which had a span of 600 mm and chord of 200 mm. The airfoil was manufactured in one piece using the additive manufacturing technique of Selective Laser Sintering (SLS) from polyamide. The airfoil was designed to be highly instrumented for the measurement of both aerodynamic and aeroacoustic phenomena in the form of static pressure and unsteady surface pressure. Instrumentation was achieved by the use of brass tubes which were installed with 2 part epoxy resin and smoothed to the surface of the airfoil. In total there were 48 static pressure taps and 88 unsteady surface pressure taps which were drilled with a 0.4 mm bit to avoid pressure attenuation at high frequencies. The surface pressure taps were connected in a remote sensing configuration using Panasonic WM-61A microphones, more information regarding this measurement technique is in the literature[37,38]. All microphones were calibrated in both magnitude and phase referenced to a single GRAS 40PL microphone, which was calibrated using a GRAS 42AA pistonphone calibrator. Unsteady surface pressure measurements made via remote sensing were sampled at 2^{15} Hz for 32 seconds. Static pressure measurements were obtained from two Chell MicroDaq-32 pressure acquisition systems and were sampled for 32 seconds at 1000 Hz.

B. far-field measurement

The turbulence interaction noise was measured using the facilities far-field microphone array, see Fig. 1. The array consists of 23 microphones arranged at 5° increments between

TABLE I. Properties of the porous structures used in the leading edge

Porosity, φ (%)	Minimum pore diameter, d_{pore} (mm)	Permeability, κ
40	0.58	2.78×10^{-9}
50	1.48	3.78×10^{-9}
60	2.29	4.98×10^{-9}

polar angles of $\theta = 35°$ and $150°$ to allow for directivity measurements. The arc was located 1.75 m above the airfoil and the microphone at $90°$ was located directly above the leading edge of the airfoil. The microphones on the arc were 1/4 inch GRAS 40PL microphones, which exhibit a flat frequency response for a large dynamic range of 10 Hz and $20,000$ Hz. All microphones were calibrated using a GRAS 42AA pistonphone calibrator prior to the experiments.

C. Turbulence grids

To generate the incoming turbulence, a grid was placed within the contraction nozzle of the wind tunnel, as shown in Fig. 1. The position of the grid within the tunnel was shown to not affect the normal background jet noise of the wind tunnel[39], thus allowing for direct noise measurement of the interaction noise between the turbulent flow and NACA

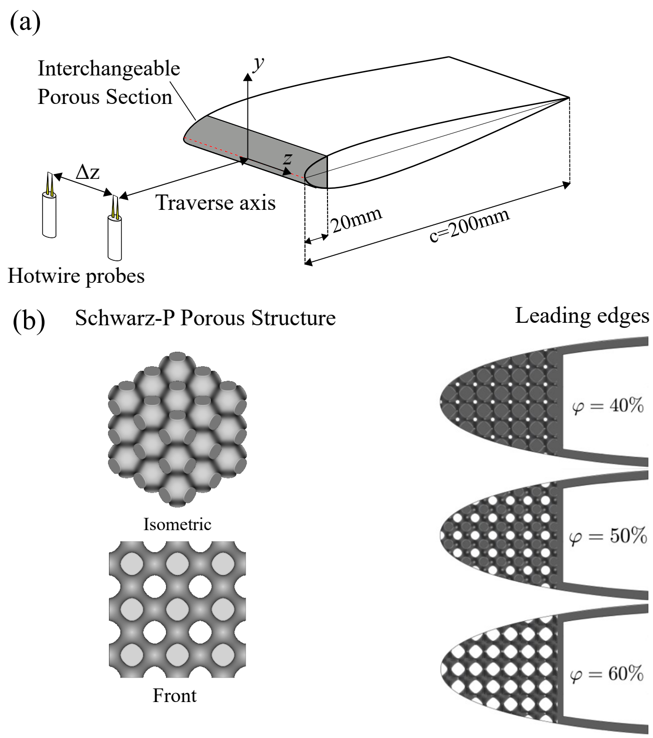

FIG. 2. NACA 0012 airfoil with interchangeable leading edge for both solid and porous leading edges, schematic of tandem hot-wires and a schematic of the Schwarz-P porous structure.

0012 airfoil with various porous leading edges. The geometric properties and generated flow properties of the grid are outlined in Table II.

D. Porous leading edges

Figure 2(a) illustrates a schematic of the airfoil. The first 20% of the leading edge was interchangeable, between a solid, instrumented leading edge and the 3D printed porous leading edges. Three different porous leading edges, with porosity of $\varphi = 40\%$, 50% and 60% were selected to study the effect of porosity on the reduction of leading interaction noise. The porous structure is based on the Triply periodic minimal Schwarz-P surface

TABLE II. The geometric properties of the grid, and the flow properties at the position of contraction nozzle exit, $x = 0$, at a freestream velocity $U_\infty = 20$ m/s. The definitions of d and M can be found on Fig. 1.

Diameter, d (mm)	Mesh, M (mm)	σ	Turbulence intensity (%)	Integral length scale (mm)
45	233	0.35	10.1	10.8

which occupied the first 10% of the airfoil chord, see Fig. 2(b). The porous leading edge was printed using a FormLabs Form3 stereolithography (SLA) printer. The tested structures were characterized prior to the tests for both porosity and permeability, and are provided in Table I. The porosity of each sample is predefined in CAD software and verified by the mass of the 3D printed structure. The airflow permeability of the structure was defined by measuring the pressure drop across each sample in a permeability rig, a more detailed procedure of this test is previously presented[40].

E. Hot-wire anemometry setup

The flow field upstream of and around the leading edge was characterized by Constant Temperature Anemometry (CTA) measurements. Two Dantec 55P16 single-wire probes were used in tandem configuration to obtain two-point correlations in front of the leading edge of the airfoil, as shown in Fig. 2. A Dantec 55P61 minature x-wire probe was utilized to measure the flow field near to the surface of the airfoil leading edge. All probes were operated using a Dantec Streamline Pro system with a CTA91C10 module with a low-pass filter of 30 kHz. The data were acquired using a National Instruments PXIe-4499 module mounted in a National Instruments PXIe-1026Q chassis. All hot-wire measurements were sampled at a rate of 2^{15} Hz for a duration of 16 seconds. The data from two-point correlation measurements using tandem hot-wire probes was sampled simultaneously. All hot-wire probes were calibrated daily using a Dantec 54H10 calibrator. Furthermore, the x-wire probe was calibrated for yaw angles between -40° and 40°. The uncertainty of the velocity measurement was estimated as 2.72% for a free-stream velocity of 20 m/s. The tandem hot-wire probes, used for spanwise coherence studies, were traversed using a ThorLabs LTS300 300 mm Translation Stage with stepper motor along the x-axis with a positioning accuracy of ± 5 μm. The tandem probes were arranged along the z-axis directly upstream of the airfoil leading edge, see Fig. 2b. The probes were traversed upstream of the airfoil leading edge to acquire measurements at 35 streamwise locations covering the region -100 mm$< x < -0.03$ mm, corresponding to $-31.51 < x/r < -0.01$, where r is the leading edge radius of the airfoil. Two-point correlations for a broad range of separation distances were obtained with repeated traverse measurements with the separation distance ranging between 5.3 mm $< z <$ 27 mm, corresponding to $1.67 < \Delta z/r < 6.40$. The x-wire probe was traversed using two connected ThorLabs LTS300 for movement in both the x-axis and y-axis.

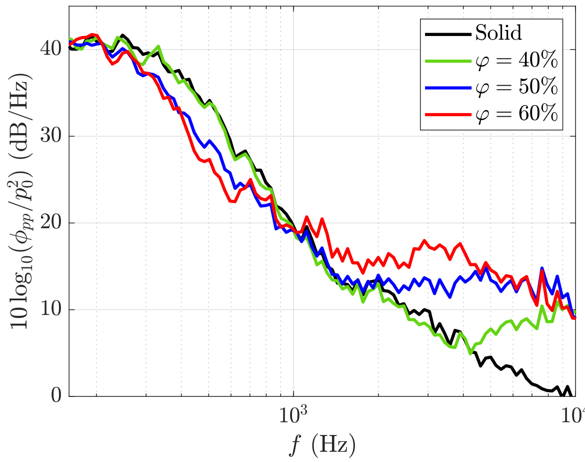

FIG. 3. Far-field noise generated by the NACA 0012 airfoil with a solid and porous leading edge immersed in the turbulent flow generated by the grid and measured by the microphone at $\theta = 90°$ directly above the leading edge.

III. RESULTS

A. Far-field noise analyses

The far-field noise of the NACA0012 airfoil with solid and porous leading edges in the flow generated by a turbulence grid are presented in this section. The presented results are for a single flow velocity of $U_\infty = 20$ m/s, with a turbulence intensity of 10.1% and integral length scale of $\Lambda = 10.8$ mm. The section considers the power spectral density level (PSD) of the far-field noise observed at different polar angles, see Fig. 1, over the frequencies 160 Hz$< f < 10,000$ Hz. This is calculated using $10 \cdot \log_{10}(\phi_{pp}/p_0^2)$, where ϕ_{pp} is the power spectral density of the measured acoustic pressure and p_0 is the reference pressure of 20 μPa. Secondly, the overall sound pressure level is presented and the directivity of the radiated

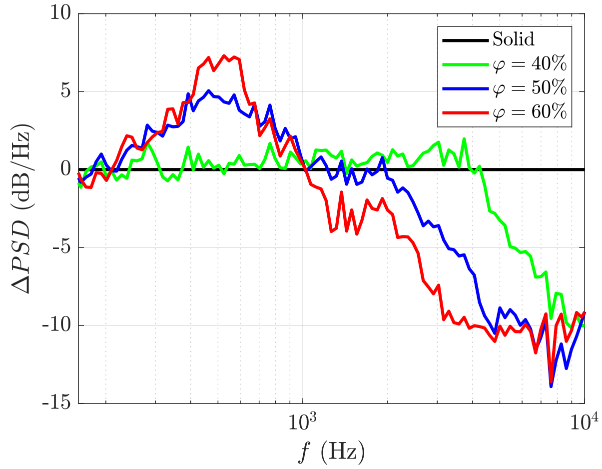

FIG. 4. Comparison of the Far-field noise reduction obtained by each porous leading edge compared to the solid leading edge immersed in the turbulent flow generated by the grid and measured by the microphone at $\theta = 90°$ directly above the leading edge.

noise is considered. The overall sound pressure level is calculated as,

$$OASPL = 10 \cdot \log_{10} \left[\frac{\int \phi_{pp}(f) \, \mathrm{d}f}{p_0^2} \right], \tag{1}$$

integrating the energy spectrum with respect to frequency, between 160 Hz$< f <$ 20,000 Hz. It should be noted that the turbulence interaction noise of the airfoil is significantly higher than the normal background noise of the wind tunnel jet between the frequencies 160 Hz $< f <$ 1000 Hz. For frequencies between 1000 Hz $< f <$ 10,000 Hz interaction noise is not observed, and the airfoil noise generated by the NACA0012 airfoil is comparable to the background noise of the facility. Both observations are previously demonstrated[39].

First, we consider the airfoil turbulence interaction noise measured by the microphone on the array at polar $\theta = 90°$, positioned directly above the leading edge. Figure 3 shows the comparison between the noise spectra of the NACA0012 airfoil with a solid and porous

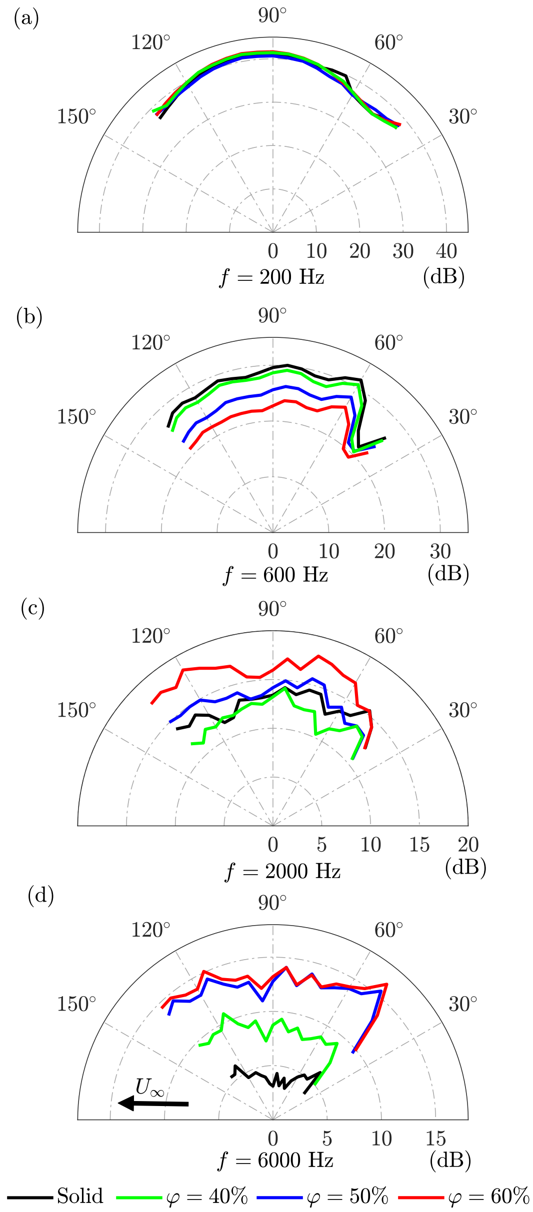

FIG. 5. Directivity of PSD level of the noise for the solid and porous leading edge cases measured by the microphone array and presented for frequencies (a) $f = 200$ Hz, (b) $f = 600$ Hz, (c) $f = 2000$ Hz and (d) $f = 6000$ Hz.

leading edges, plotted against narrowband frequency. When comparing the results of the porous leading edges to those of the solid leading edge, it can be seen that porosity plays an important role on the level of noise reduction that is achieved. Considering the results of the leading edge of porosity $\varphi = 40\%$, there is little-to-no noise reduction over the frequency range where turbulence interaction noise is observed, i.e. 160 Hz $< f <$ 1000 Hz. An increase in the porosity of the leading edge results in a reduction of the observed turbulence interaction noise, where the greatest reduction is for the $\varphi = 60\%$ leading edge. The results show that increasing the porosity of the leading edge structure can further reduce the turbulence interaction noise. However, it is clear from Fig. 3 that the porous leading edge results also demonstrate a noise increase at higher frequencies i.e. $f > 1000$ Hz. An increase in the porosity of the leading edge structure enhances the high frequency noise generation. This high frequency noise generation is previously shown to be caused by the flow interacting with the rough porous structure[20] and can be reduced with the introduction of a cover over the porous material[41]. Although the high frequency noise increase in the case of the porous leading edge results is significant compared to the results of the solid airfoil leading edge, the noise increase is observed at a much lower PSD level than the noise reduction.

A clearer performance of the noise reduction achieved by each porous leading edge is provided by Fig. 4, where the far-field noise data is presented as $\Delta PSD = PSD_{solid} - PSD_{porous}$ and a positive value denotes noise reduction. As can be seen in Fig. 4, the use of a $\varphi = 60\%$ porous treatment can lead to a noise reduction of up to 7 dB over 400 Hz $< f <$ 700 Hz. Observed noise reduction for the leading edge with a porous treatment of $\varphi = 50\%$ peaks at 5 dB for the frequency range 400 Hz $< f <$ 600 Hz. Furthermore, both leading edges of porosity $\varphi = 60\%$ and $\varphi = 50\%$ demonstrate noise reduction between 160

Hz $< f <$ 1000 Hz. Interestingly, the porous leading edge of porosity $\varphi = 40\%$ shows no significant noise reduction over 160 Hz $< f <$ 4000 Hz. High frequency noise increase is evident in the results of each porous leading edge, however the frequency of where the noise increase is evident varies with porosity.

To assess the potential changes to the mechanism that causes the turbulence interaction noise as a result of employing porous leading edges, the directivity of the sound at multiple frequencies has been considered. A significant change to the directivity patterns between the solid and porous cases may signify a change to the noise generation mechanism. Figure 5 presents the results of the directivity of the PSD level for the solid and porous leading edge cases at four chosen frequencies, namely f = 200 Hz, 600 Hz, 2000 Hz and 6000 Hz, at a freestream velocity of U = 20 m/s. The frequencies were chosen to cover the low frequencies (160 Hz$< f <$ 1000 Hz), where turbulence interaction is dominant, the cross-over frequency (f = 2000 Hz), where little or no noise change was observed, and high frequencies (2000 Hz$< f < 10,000$ Hz), where the significant noise increase due to surface roughness is observed. The results of directivity of the radiated noise for f = 200 Hz are presented in Fig. 5(a) and demonstrate no change in the directivity pattern between the solid and porous leading edge cases. At the frequency f = 600 Hz, the results show a reduction of up to 7 dB in the radiated noise from the airfoils fitted with a porous leading edge. Between the polar angles $60^\circ < \theta < 135^\circ$, the reduction of the PSD becomes more substantial as the porosity increases, although there is little change to the pattern of the radiated noise. Furthermore, Between polar angles $40^\circ < \theta < 60^\circ$ there is less significant reduction of the PSD between the results of the solid and porous leading edges. At the crossover frequency (f = 2000 Hz), the directivity pattern of the solid and porous cases exhibit some differences, despite the comparable levels of PSD exhibited in Figs. 3 and 4. At high frequencies, i.e. $f = 6000$ Hz, where the roughness noise is believed to be the dominant noise source in the case of the porous leading edges, the directivity patterns are significantly different to that of the solid leading edge, signifying the changes to the noise generation mechanism.

The overall sound pressure level (OASPL) results assesses the directivity pattern of the noise generated by the solid and porous leading edge cases. As the OASPL calculation integrates the PSD level across the narrowband spectrum, the OASPL results include each porous leading edge's contribution to the low frequency noise reduction and the subsequent noise increase at higher frequencies too. Figure 6 presents the OASPL results of the NACA0012 airfoil turbulence interaction noise with solid and porous leading edges at a freestream velocity of $U = 20$ m/s. The directivity results of the solid and porous leading edges are comparable across the polar angles presented. The maximum level of OASPL noise reduction is approximately 3 dB and is achieved by the leading edge of porosity $\varphi = 60\%$, between the polar angles of $65° < \theta < 100°$. It is clear that when considering the full noise spectrum, the reduction of the turbulence interaction noise achieved using the porous leading edge far outweighs the roughness noise increase observed at high frequency, see Fig. 4. Considering the OASPL results of the solid case compared to the porous cases, it is clear that the leading edge with porosity $\varphi = 40\%$ shows little noise reduction. Interestingly, both the result of $\varphi = 50\%$ and $\varphi = 60\%$ demonstrate comparable results for OASPL. Aside from the reduction in the porous cases, there is no significant change to the directivity pattern between the cases.

It is understood from the assessment of the far-field noise that the introduction of a porous leading edge reduces the turbulence interaction noise generated by the airfoil. To understand the physical mechanism responsible for the reduction of the far-field noise, the flow field upstream of and around the airfoil must be examined.

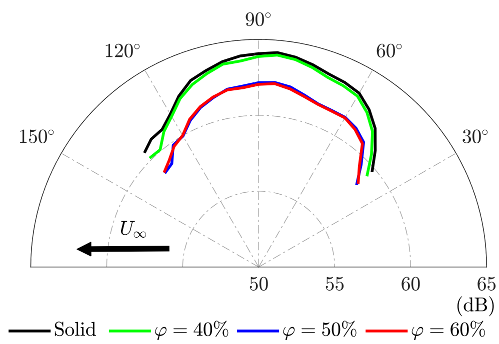

FIG. 6. Directivity of the OASPL for the NACA 0012 airfoil with both solid and porous leading edges.

B. Flow field analyses

Detailed flow measurements of the region in front of and around the leading edge of the airfoil were carried out to quantify flow field differences between the solid and porous leading edges, using single-wire and two-component x-wire hotwire probes. Flow field analyses are presented for a grid flow with a turbulence intensity of 10.1% and integral length scale of $\Lambda = 10.8$ mm, at the free-stream velocity of $U_\infty = 20$ m/s. Figure 7 presents the vectors of velocity results for the solid and porous leading edge cases for a freestream velocity of $U_\infty = 20$ m/s. Each arrow is representative of the resultant velocity vector, measured by the x-wire probe at each location. The results of the solid case demonstrate the flow deflection caused by the airfoil near the leading edge (i.e. $-0.01 < x/c < 0.05$) and the velocity vectors following the airfoil shape further downstream of the leading edge (i.e. $0.05 < x/c < 0.25$). The velocity results in the vicinity of the surface of the airfoil shows no significant difference to the magnitude of the arrows further from the airfoil surface, signifying that the measurements for the solid case are taken outside the boundary layer. The results of the porous leading edge cases show that the flow penetrates into the porous leading edge region, represented as the arrows near the leading edge with a lower vertical velocity component (i.e. more horizontal). The flow penetration into the porous leading edge is more evident in the region $-0.01 < x/c < 0.1$. The main differences between the flows of each case are evident in the vectors closest to the surface of the airfoil, where increased porosity generates a larger velocity deficit close to the surface. This result helps to highlight the flow penetration into the porous leading edges which a single-wire probe is unable to capture.

As previously shown[32,42], the flow structures undergo significant changes in close proximity of the stagnation point, before impinging on the airfoil. Given the spatial constraint, and also need for resolving high frequencies, such flow measurements can only be achieved using single-wire probes. Detailed flow measurements upstream of the airfoil leading edge, obtained with the use of a single-wire hotwire probe, reveal interesting behavior for the porous leading edge cases in the vicinity of the leading edge (i.e. $-1.5 < x/r < -0.01$). Figure 8 presents the results of velocity measurements upstream of the leading edge of the solid and porous airfoil leading edges over a wide spacial range, i.e. $-5 < x/r < -0.01$. Figure

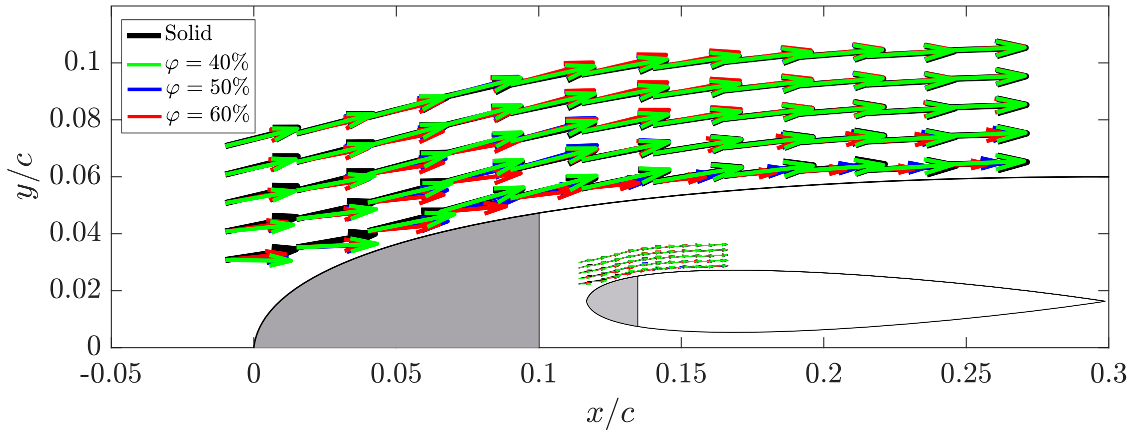

FIG. 7. Vectors of velocity magnitude over the leading edge region of the airfoil for both the solid and porous leading edge case measured by CTA cross-wire probe.

8(a) presents the mean-flow velocity normalized by the freestream velocity (U/U_∞) for the solid and porous leading edge cases. The mean-flow velocity results of the solid leading edge demonstrate a reduction in the velocity approaching the leading edge of the airfoil, caused by the velocity stagnation of the solid airfoil leading edge. This result is expected and consistent with the literature[32]. When comparing the solid and porous leading edges results, all results demonstrate comparable behavior for the region $-5 < x/r < -1.5$. In the case of solid leading edge, the stagnation effect is evident by a sharp decay in the total velocity along the stagnation streamline between $-1.5 < x/r < -0.01$. However, the stagnation effect for the porous leading edges is dramatically reduced, which signifies the presence of flow penetration into the porous volume. It should be noted that unlike the solid leading edge results, there is an acceleration of the flow close to the porous leading edges which is exacerbated by decreasing porosity.

Turbulence interaction with an external body can cause significant changes to the turbulence intensity of the flow in the proximity of the body[32,42]. The presence of a porous structure and potential flow penetration into the porous volume can further complicate the evolution of the turbulent structures upstream of the external body. Figure 8(b) presents the root-mean-square (rms) of the velocity fluctuation normalized by the rms of freestream velocity fluctuation for both the solid and porous leading edge cases. The results of the solid leading edge demonstrate a reduction in the rms of velocity fluctuation approaching the leading edge within $-5 < x/r < -0.25$. In proximity to the leading edge, i.e.$-0.25 < x/r < -0.01$, there is a sudden increase in the velocity fluctuation which is caused by redistribution of the velocity fluctuation from the streamwise direction to the crosswise, known as upwash[32]. Comparing the results of the solid and porous cases, again, a comparable behavior is observed for the region $-5 < x/r < -1.5$. In the region where the solid leading edge results experiences a reduction, followed by a sudden recovery of the rms of velocity fluctuation, the porous leading edges results demonstrate a significant increase in the rms of velocity fluctuations, inside $-1.5 < x/r < -0.01$. As shown in Fig. 8(b), in the case of the solid leading edge, the rms of velocity fluctuation reaches its minimum at $x/r = -0.15$, while that for the $\varphi = 60\%$ has moved to the location $x/r = -0.8$. The position of the minimum value of rms of velocity fluctuation moves further upstream from the leading edge as the porosity decreases. For $\varphi = 60\%$, 50% and 40% the location of the rms of velocity increase is $x/r \approx -0.8$, -1 and -1.5, respectively. Furthermore, as porosity decreases, the level of the velocity fluctuation rms at the leading edge significantly increases. This is an interesting result, and contrasts to the previous observation in the literature[32].

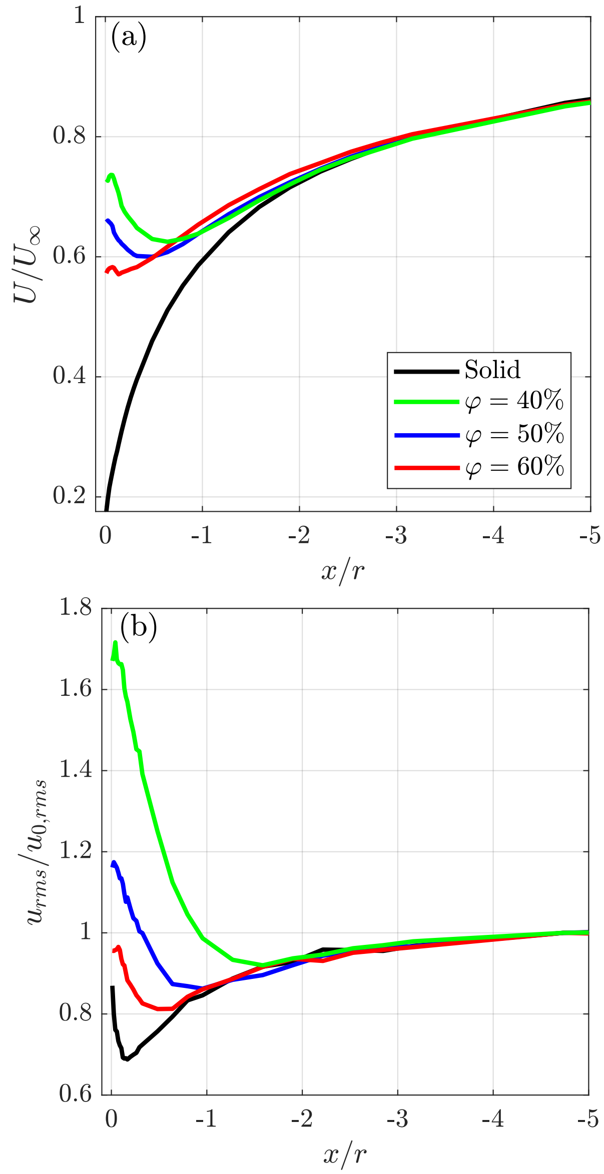

FIG. 8. Stagnation streamline flow properties measured by single-wire probe for *(a)* normalized flow velocity (U/U_∞) and *(b)* normalized velocity fluctuation ($u_{rms}/u_{0,rms}$) for the solid and porous leading edge cases.

To understand the energy content of the velocity fluctuations along the stagnation streamline, the power spectral density level of the velocity fluctuations has been calculated and is presented in two forms. The first, is the standard presentation that is used as an input for noise prediction models i.e. Amiet[1], which is the PSD level of the velocity fluctuations, calculated as $10\log_{10}(\phi_{uu}/u^2_{0,rms})$. The second, is the pre-multiplied energy spectra, where the pre-multiplied energy spectra is presented and the total area under the curve is representative of the total energy at each location. The remaining results presented in this paper are a comparison between the solid case and the porous leading edge of porosity $\varphi = 50\%$ for the sake of brevity. Figures 9(a) and 9(c) presents the PSD level of velocity fluctuations for the solid and porous leading edge cases and figures 9(b) and 9(d) presents the pre-multiplied energy spectra of velocity fluctuations for the solid and porous leading edge cases. The PSD level of velocity fluctuations results for the solid case demonstrate an interesting behavior. At the freestream measurement location, there is a consistent value of PSD level of velocity fluctuation, a turning point at $f = 60$ Hz, and a consistent decay gradient of $f^{-5/3}$ between 100 Hz$< f <$ 2000 Hz signifying freely-decaying turbulence of the inertial subrange. Up to $x/r = -0.33$, there is a reduction in the low frequency content in the PSD of velocity fluctuation (i.e. $f < 100$ Hz), coupled with a reduction at very high frequency (i.e. $f > 2000$ Hz). However, no change to the $f^{-5/3}$ decay range is observed. In proximity of the leading edge ($-0.15 < x/r < -0.01$), there is a recovery to the low frequency energy content of the velocity fluctuation, accompanied by a reduction of the velocity energy contact at high frequencies. When comparing the PSD level of velocity fluctuation along the stagnation streamline for the solid and porous leading edge, see figures 9(a) and 9(c), a more apparent change in both the low and high frequency behavior is evident in the porous leading edge case. The dissimilarity of the PSD of velocity fluctuations between the results of the solid and porous leading edge cases are more evident in the region close to the leading edge, i.e. $-0.96 < x/r < -0.01$. The low frequency increase in the PSD of velocity fluctuations, evident within $-0.33 < x/r < -0.01$, exceeds the low frequency levels measured at the freestream, i.e. $x/r = -33$. Furthermore, there is an emergence of a broadband hump which peaks at $f = 70$ Hz. When considering the high frequency decay gradients, the results of the solid case show no significant deviation from the $f^{-5/3}$ decay gradient between the frequency range 100 Hz$< f <$ 2000 Hz. However, velocity PSD results for the porous leading edge case show the high frequency decay gradient increases along the stagnation streamline approaching the leading edge. The change to the high frequency decay of the velocity fluctuation is a significant observation as this phenomenon signifies external contribution to the change of the small scale turbulent structures approaching the porous leading edge.

The pre-multiplied energy spectra accentuates the variations between the cases as the total area under each curve is representative of total energy and are presented in Figs. 9(b) and 9(d). The pre-multiplied energy spectra results offer more insight into the nature of the velocity fluctuation along the stagnation streamline, presented in Fig. 8. The pre-multipled energy spectra results for the solid leading edge show the reduction of energy up to $x/r = -0.15$ and sudden recovery at $x/r = -0.01$ is more clear. The pre-multiplied energy spectra of velocity fluctuation results of the solid leading edge appear to lose more low frequency energy up to $x/r = -0.15$, as the peak of the curve reduces and shifts to a higher frequency. At the stagnation point, $x/r = -0.01$, there is some recovery of the velocity fluctuation energy level but it remains lower than that of the freestream flow ($x/r = -33$). As can be seen in Fig. 9(d), the porous leading edge results are dramatically different from those of the solid case. It is clear in the results of the pre-multipled energy spectra that the behavior far upstream of the leading edge, i.e. $x/r = -4.74$ and -0.96, is comparable between the solid and porous cases. Closer to the leading edge, at $x/r = -0.33$, the energy level of the velocity fluctuations remain comparable to that of the freestream level, but with the emergence of a distinct peak at about $f = 70$ Hz. In the proximity of the leading edge ($x/r = -0.01$), the energy level is seen to further increase around $f = 70$ Hz, with the most energetic turbulent scales concentrated between 40 Hz$< f <$ 300 Hz.

The energy spectra data presented here provides insight to the energy level of the flow structures for the solid and porous leading edge cases, showing significant dissimilarities between the cases in close proximity to the leading edge. However, we still need to gain an understanding of the physical size and changes to the shape of the turbulent structures as the approaching the airfoil leading edge, this is further explored in the next section with the analysis of two-point correlation upstream of the leading edge.

C. Two-point correlation analysis

The two-point correlation of the velocity fluctuations along the stagnation streamline, schematically illustrated in Fig. 2, offers information on the level of coherence of the flow structures and their physical size in the spanwise direction. By performing several two-probe coherence studies at different streamwise locations upstream of the leading edge, one can study the changes to the size of the turbulent flow structures as they approach the airfoil

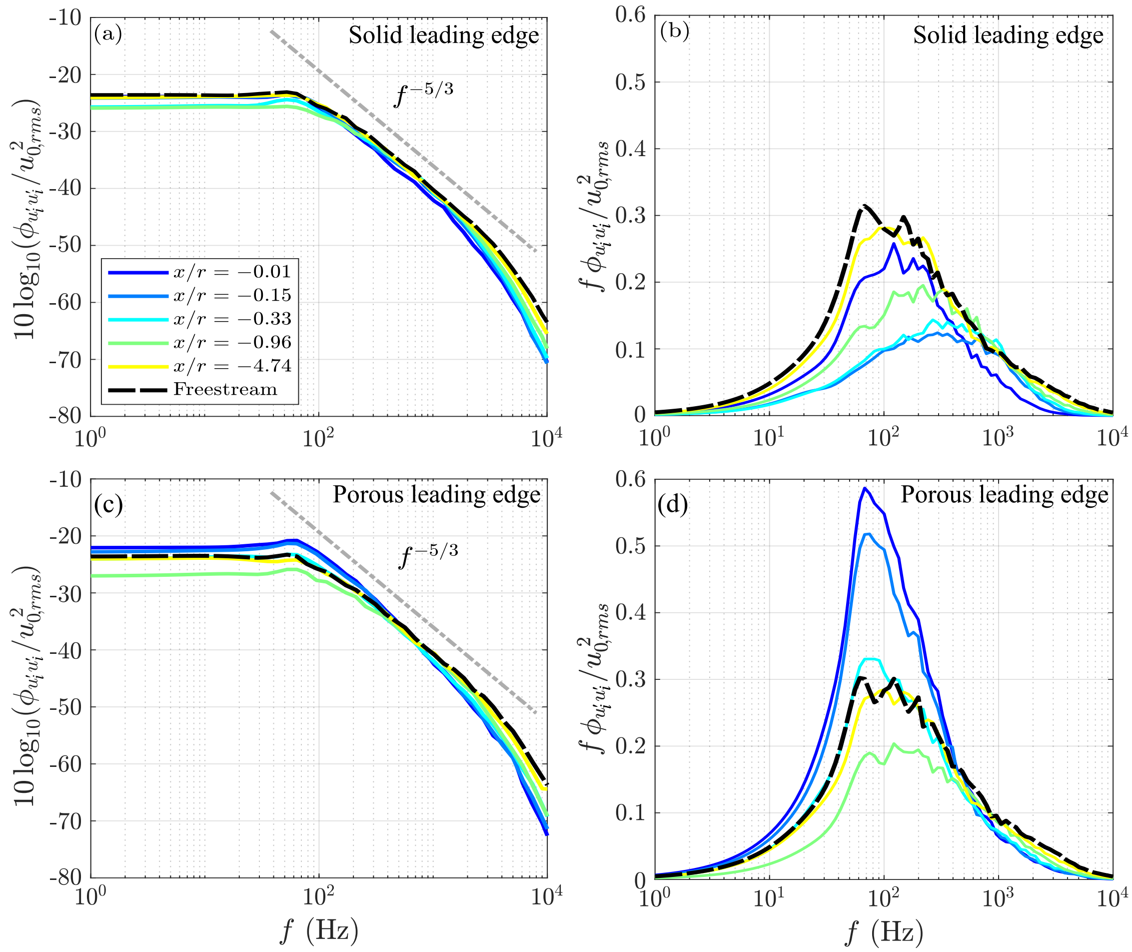

FIG. 9. Energy spectrum analysis of velocity fluctuation along the stagnation streamline upstream of the NACA 0012 aerofoil leading edge between $-4.74 < x/r < -0.01$ where (a) and (c) are the PSD and pre-multiplied PSD of the solid leading, (b) and (d) are the PSD and pre-multiplied PSD of the porous leading edge ($\varphi = 50\%$).

leading edge. The magnitude-squared of the spanwise coherence is calculated as

$$\gamma^2_{u_i' u_j'}(f, \Delta z) = \frac{\left|\phi_{u_i' u_j'}(f)^2\right|}{\left|\phi_{u_i' u_j'}(f)\right|\left|\phi_{u_i' u_j'}(f)\right|}, \tag{2}$$

where $\gamma^2_{u_i' u_j'}(f, \Delta z)$ is the spanwise coherence calculated between two single-wire probes in a tandem configuration, separated by Δz, and $\phi_{u_i' u_j'}$ denotes the cross-power spectral density between the two probes i and j, respectively. Figure 10 presents the results of the spanwise coherence of the velocity fluctuation for the flow along the stagnation streamline for the case with the solid leading edge at different upstream locations (freestream, $x/r = -4.74$, -0.96, -0.33, -0.15 and -0.01), and for a wide range of probe separations ($\Delta z/r = 6.40$, 4.16, 2.68, 2.11, and 1.67). Considering the spanwise coherence results for the freestream case (Fig. 10(a)), there appears to be a strong level of coherence at frequencies 10 Hz$< f <$ 100 Hz, for small spanwise separation distance ($\Delta z/r = 1.67$), which steadily decays up to $f = 1000$ Hz. The level of coherence at low frequency (i.e. $f < 1000$ Hz) systematically decreases as the spanwise separation increases to $\Delta z/r = 6.40$. At the far upstream location ($x/r = -4.74$), see Fig. 10(b), there is still a high level of spanwise coherence of the velocity fluctuation evident, although there is a reduction in the magnitude, particularly at the highest spanwise separation ($\Delta z/r = 6.40$). As seen, the results at the far upstream locations ($x/r = -4.74$) in Fig. 10(b), are very similar to those observed in the freestream cases in Fig. 10(a). In Fig. 10(c), a further reduction in the level of spanwise coherence of velocity fluctuation is evident at $x/r = -0.96$, however there is still sensitivity to the increase of spanwise separation. At locations closer to the leading edge, up to $x/r = -0.33$, there is an overall reduction in the spanwise coherence of the velocity fluctuations, and the coherence becomes less dependent on the spanwise spacing (Δz), indicating the emergence of more two-dimensional flow structures. Approaching the stagnation, at $x/r = -0.15$, the coherence begins to increase, compared to $x/r = -0.33$. The coherence level further increases in the imminent upstream region of the leading edge between $x/r = -0.15$ and $x/r = -0.01$. Furthermore, there is the emergence of a dominant peak in the spanwise coherence of the velocity fluctuation for all separations which is centered at $f \approx 70$ Hz. As mentioned earlier, the sensitivity of the two-point velocity coherence to spanwise separation distance (Δz) is gradually lost moving towards the airfoil leading edge which can be interpreted as the turbulent structures becoming more two-dimensional. This behavior represents the turbulent structures distorting and rolling up over the leading edge of the airfoil.

Figure 11 presents the results of the spanwise coherence of the velocity fluctuations for the flow along the stagnation streamline between $-4.74 < x/r < -0.01$ for the case with the porous leading edge. As the same turbulent flow is generated in both leading edge cases, the freestream results for the solid and porous cases are the same. As previously shown in Fig. 8, the results of the velocity and rms of velocity fluctuation for the solid and $\varphi = 50\%$ porous leading edges exhibit the same behavior between $-4.74 < x/r < -0.96$. This is echoed in the spanwise coherence results for the same region, as the same results are evident for the solid case (Figs. 10(b) and (c)) as in the porous case (Figs. 11(b) and (c)), respectively. For the porous leading edge case there is a reduction in the spanwise coherence approaching $x/r = -0.96$ which corroborates with the results of the solid leading edge. Moving close to the leading edge ($x/r = -0.33$), disparities in the coherence results between the solid and porous leading edge cases appear inside one leading edge radius of the leading edge, i.e. Figs 10(d) and 11(d), as the spanwise coherence of the velocity fluctuations begin to increase. The level of spanwise coherence of velocity fluctuations is more significant for the porous than that of the solid case. While the coherence results of the porous case show some level of spanwise distance dependency, this is weaker than the freestream turbulent flow further upstream, indicating the emergence of more two-dimensional turbulent structures in the vicinity of the leading edge. In the proximity of the leading edge, i.e. $x/r = -0.01$, the level of spanwise coherence of the velocity fluctuation further increases to exceed the freestream level for all separations. In addition, the dominant peak of $f \approx 70$ Hz, evident in Figs. 9(c) and 9(d), remains a prominent feature for all spanwise separation distances at $x/r = -0.01$. The higher level of coherence coupled with the increased energy level of the turbulent structures at close proximity to the leading edge demonstrates that the porous leading edge significantly changes the behavior of the flow close to the leading edge of the airfoil.

The flow field and two-point correlation analyses demonstrate how a turbulent flow upstream of the airfoil leading edge can be altered by the introduction of the porous treatment over the leading edge area. Furthermore, the variation in the leading edge porosity between $\varphi = 40\%$ and $\varphi = 60\%$ is shown to result in strong changes to the energy content of the velocity fluctuations upstream of the leading edge. However, it should be noted that the presented results only cover a single turbulent inflow condition. The underlying physics of turbulence interaction noise is believed to be dependent on the turbulent characteristics of the inflow, specifically the turbulent intensity and integral length scale[2,5,39]. To this end, the physics of the noise reduction mechanism for a porous leading edge in airfoil turbulence interaction noise is likely susceptible to the turbulent inflow conditions. Future works will focus on better understanding of flow distortion around porous leading edges in turbulent flows with a range of turbulence intensities and integral length scales.

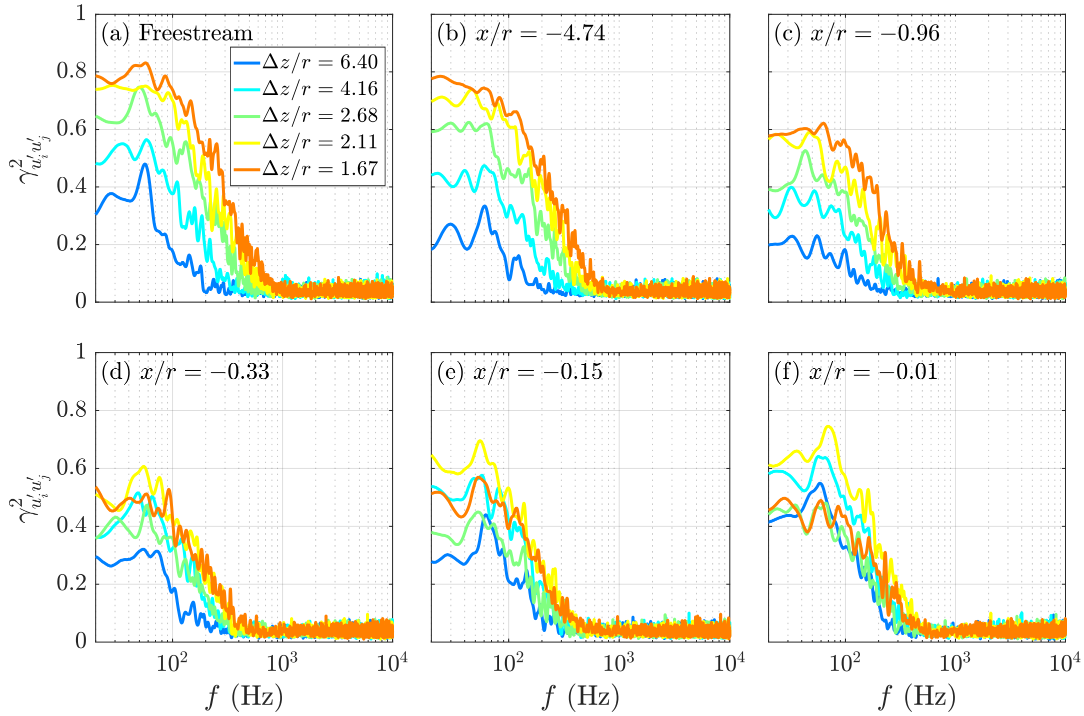

FIG. 10. Spanwise magnitude-square coherence ($\gamma^2_{u'_i u'_j}$) of velocity fluctuation measured by tandem hot-wire probes at multiple spanwise separations ($\Delta z/r$) for solid leading edge along stagnation streamline.

IV. CONCLUSION

This paper presents a study on airfoil turbulence interaction noise reduction using a porous treatment at the leading edge. The study implements a NACA 0012 airfoil of chord $c = 200$ mm which interacts with a turbulent flow, generated by the means of a passive turbulence grid. The leading edge part of the airfoil is interchangeable between a solid leading edge and a porous leading edge. The structure utilized at the leading edge is a Schwartz-Primitive Triply periodic minimal structure. The porosity of the leading edge is varied between three values of porosity $\varphi = 40\%$, 50% and 60% to alter the bulk materials'

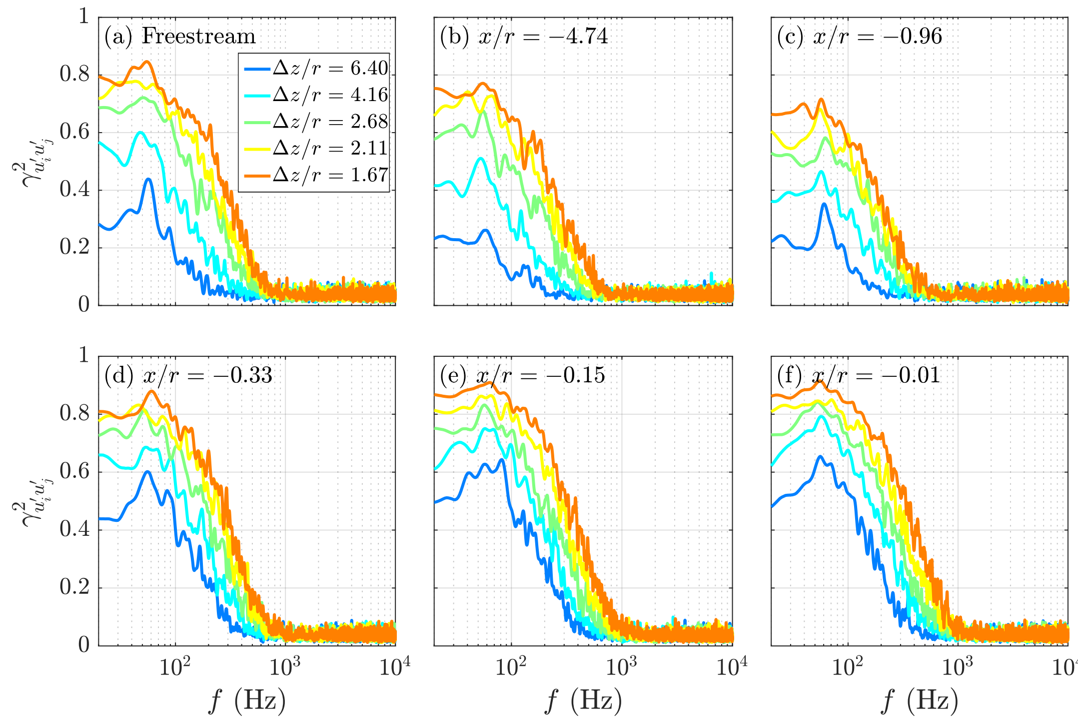

FIG. 11. Spanwise magnitude-square coherence ($\gamma^2_{u'_i u'_j}$) of velocity fluctuation measured by tandem hot-wire probes at multiple spanwise separations ($\Delta z/r$) for porous leading edge ($\varphi = 50\%$) along the stagnation streamline.

permeability. Variation of the porosity and permeability of the leading edges was studied to understand their effect on turbulence interaction noise. Far-field noise results suggested that increasing the porosity results in more effective low-frequency noise reduction, with the penalty of high-frequency noise increase. The use of a porous leading edge with a porosity of $\varphi = 40\%$ showed little noise reduction compared to the solid leading edge, whereas 50% and 60% demonstrated significant noise reduction at low frequencies. The overall sound pressure level results revealed little variation in the directivity of the noise between the solid and porous leading edges, and the overall sound pressure level results between the $\varphi = 50\%$ and 60% cases offer comparable noise reduction. Analysis of the flow field by the means of CTA hot-wire measurements revealed flow penetration into the porous leading edges, with increasing porosity showing a velocity deficit close to the wall of the airfoil. An interesting behavior is observed for measurements along the stagnation streamline, when approaching the leading edge of the airfoil a rapid increase in the rms of velocity fluctuation is evident, contrary to previous experimental observations. The analysis of the PSD of velocity fluctuations confirmed a significant increase in the energy level close to the porous leading edge which contradicts the current experimental literature. Further numerical and experimental investigations are needed to understand whether the increase in energy is due to the redistribution of energy from streamwise to crosswise, or due to the nature of the hydrodynamic penetration of the flow in the porous leading edge. Two-point spanwise velocity fluctuations coherence analysis revealed that approaching the leading edge of the airfoil the solid case generates a 2D structure due to the loss of separation sensitivity between the hotwires. For the porous leading edge, it is evident that spanwise coherence of the velocity fluctuations increases near the porous leading edge and exceeds the freestream level.

ACKNOWLEDGMENTS

The first author (L.B.) would like to acknowledge the financial support of Embraer S.A. and an Engineering and Physical Sciences Research Council doctoral training partnership (EPSRC DTP). The second author (A.C.) was sponsored by EPSRC via Grant No.

EP/S013024/1 at the University of Bristol from 1/6/2020 to 1/12/2022. All authors would like to acknowledge the financial support of EPSRC via Grant No. EP/S013024/1.

REFERENCES

[1]R. Amiet, "Acoustic radiation from an airfoil in a turbulent stream," Journal of Sound and Vibration **41**(4), 407 – 420 (1975) doi: https://doi.org/10.1016/S0022-460X(75)80105-2.

[2]R. Paterson and R. Amiet, "Acoustic radiation and surface pressure characteristics of an airfoil due to incident turbulence," Proceedings of the 3rd Aeroacoustics Conference, Palo Alto, CA, AIAA-76-571 (1976).

[3]S. Moreau and M. Roger, "Effect of angle of attack and airfoil shape on turbulence-interaction noise," 11th AIAA/CEAS Aeroacoustics Conference, Monterey, CA, AIAA-2005-2973 (2005).

[4]W. J. Devenport, J. K. Staubs, and S. A. Glegg, "Sound radiation from real airfoils in turbulence," Journal of Sound and Vibration **329**(17), 3470 – 3483 (2010) doi: https://doi.org/10.1016/j.jsv.2010.02.022.

[5]F. V. Hutcheson, T. F. Brooks, and D. J. Stead, "Measurement of the noise resulting from the interaction of turbulence with a lifting surface," International Journal of Aeroacoustics **11**(5-6), 675–700 (2012) doi: 10.1260/1475-472X.11.5-6.675.

[6]J. Gill, X. Zhang, and P. Joseph, "Symmetric airfoil geometry effects on leading edge noise," The Journal of the Acoustical Society of America **134**(4), 2669–2680 (2013) doi:

10.1121/1.4818769.

[7]J. R. Gill, X. Zhang, and P. Joseph, "Effects of real airfoil geometry on leading edge gust interaction noise," 19th AIAA/CEAS Aeroacoustics Conference, Berlin, Germany AIAA-2013-2203 (2013), doi: 10.2514/6.2013-2203.

[8]J. Gershfeld, "Leading edge noise from thick foils in turbulent flows," The Journal of the Acoustical Society of America **116**(3), 1416–1426 (2004) doi: 10.1121/1.1780575.

[9]S. A. Showkat Ali, M. Azarpeyvand, and C. R. Ilário da Silva, "Trailing-edge flow and noise control using porous treatments," Journal of Fluid Mechanics **850**, 83–119 (2018) doi: 10.1017/jfm.2018.430.

[10]S. A. Showkat Ali, M. Azarpeyvand, and C. R. I. da Silva], "Trailing edge bluntness noise reduction using porous treatments," Journal of Sound and Vibration **474**, 115257 (2020) doi: https://doi.org/10.1016/j.jsv.2020.115257.

[11]X. Liu, H. K. Jawahar, M. Azarpeyvand, and R. Theunissen, "Aerodynamic performance and wake development of airfoils with serrated trailing-edges," AIAA Journal **55**(11), 3669–3680 (2017).

[12]Y. D. Mayer, B. Lyu, H. K. Jawahar, and M. Azarpeyvand, "A semi-analytical noise prediction model for airfoils with serrated trailing edges," Renewable Energy **143**, 679 – 691 (2019) doi: https://doi.org/10.1016/j.renene.2019.04.132.

[13]H. K. Jawahar, Q. Ai, and M. Azarpeyvand, "Experimental and numerical investigation of aerodynamic performance for airfoils with morphed trailing edges," Renewable Energy **127**, 355 – 367 (2018) doi: https://doi.org/10.1016/j.renene.2018.04.066.

[14]A. Celik, Y. Mayer, and M. Azarpeyvand, "An experimental aeroacoustic study on serrated trailing-edge geometries and flow misalignment effects," AIAA AVIATION 2020 FORUM, AIAA-2020-2518 (2020).

[15]A. Celik, Y. D. Mayer, and M. Azarpeyvand, "On the aeroacoustic characterization of a robust trailing-edge serration," Physics of Fluids **33**(7), 075120 (2021) doi: 10.1063/5.0054767.

[16]T. F. Geyer, A. Lucius, M. Schrödter, M. Schneider, and E. Sarradj, "Reduction of turbulence interaction noise through airfoils with perforated leading edges," Acta Acustica united with Acustica **105**(1), 109–122 (2019) doi: doi:10.3813/AAA.919292.

[17]M. Roger, C. Schram, and L. D. Santana, "Reduction of airfoil turbulence-impingement noise by means of leading-edge serrations and/or porous material," 19th AIAA/CEAS Aeroacoustics Conference, Berlin, Germany, AIAA-2013-2108 (2013).

[18]A. R. Carpio, F. Avallone, and D. Ragni, "On the role of the flow permeability of metal foams on trailing edge noise reduction," 2018 AIAA/CEAS Aeroacoustics Conference, Atlanta, GA, AIAA-2018-2964 (2018).

[19]T. Sinnige, B. D. Corte, R. De Vries, F. Avallone, R. Merino-Martínez, D. Ragni, G. Eitelberg, and L. L. M. Veldhuis, "Alleviation of propeller-slipstream-induced unsteady pylon loading by a flow-permeable leading edge," Journal of Aircraft **56**(3), 1214–1230 (2019) doi: 10.2514/1.C035250.

[20]S. A. Showkat Ali, M. Azarpeyvand, M. Szőke, and C. R. Ilário da Silva, "Boundary layer flow interaction with a permeable wall," Physics of Fluids **30**(8), 085111 (2018) doi:

10.1063/1.5043276.

[21]B. Lyu, M. Azarpeyvand, and S. Sinayoko, "Noise prediction for serrated leading-edges," 22nd AIAA/CEAS Aeroacoustics Conference, Lyon, France, AIAA-2016-2740 (2016).

[22]B. Lyu and M. Azarpeyvand, "On the noise prediction for serrated leading edges," Journal of Fluid Mechanics **826**, 205–234 (2017) doi: 10.1017/jfm.2017.429.

[23]J. Kim, S. Haeri, and P. Joseph, "On the reduction of aerofoil-turbulence interaction noise associated with wavy leading edges," Journal of Fluid Mechanics **792**, 526–552 (2016).

[24]S. Narayanan, C. Paruchuri, S. Haeri, P. Joseph, J. W. Kim, and C. Polacsek, "Airfoil noise reductions through leading edge serrations," Physics of Fluids **27**(2), 025109 (2015) doi: 10.1063/1.4907798.

[25]C. Paruchuri, P. Joseph, S. Narayanan, C. Vanderwel, J. Turner, J. W. Kim, and B. Ganapathisubramani, "Performance and mechanism of sinusoidal leading edge serrations for the reduction of turbulence-aerofoil interaction noise," Journal of Fluid Mechanics **818**, 435–464 (2017) doi: 10.1017/jfm.2017.141.

[26]K. N. Chanaud, R. and R. Sitterding, "Experiments on porous blades as a means of reducing fan noise," Journal of the Acoustical Society of America **59**, 564–575 (1976).

[27]T. Geyer, E. Sarradj, J. Giesler, and M. Hobracht, "Experimental assessment of the noise generated at the leading edge of porous airfoils using microphone array techniques," 17th AIAA/CEAS Aeroacoustics Conference (32nd AIAA Aeroacoustics Conference), Portland, OR, AIAA-2011-2713 (2011).

[28]T. Geyer, E. Sarradj, and J. Giesler, "Application of a beamforming technique to the measurement of airfoil leading edge noise," Advances in Acoustics and Vibration **2012**, 1–16 (2012) doi: 10.1155/2012/905461.

[29]E. Sarradj and T. Geyer, "Noise generation by porous airfoils," 13th AIAA/CEAS Aeroacoustics Conference (28th AIAA Aeroacoustics Conference), AIAA-2007-3719 (2007).

[30]R. Zamponi, N. V. de Wyer, and C. F. Schram, "Experimental investigation of airfoil turbulence-impingement noise reduction using porous treatment," 25th AIAA/CEAS Aeroacoustics Conference, Delft, Netherlands, AIAA-2019-2649 (2019).

[31]M. Roger and S. Moreau, "Airfoil turbulence-impingement noise reduction by porosity or wavy leading-edge cut: Experimental investigations," INTER-NOISE and NOISE-CON Congress and Conference Proceedings **253**(2), 6366–6375 (2016).

[32]R. Zamponi, S. Satcunanathan, S. Moreau, D. Ragni, M. Meinke, W. Schröder, and C. Schram, "On the role of turbulence distortion on leading-edge noise reduction by means of porosity," Journal of Sound and Vibration **485**, 115561 (2020) doi: https://doi.org/10.1016/j.jsv.2020.115561.

[33]C. Paruchuri, P. Joseph, T. P. Chong, M. Priddin, and L. Ayton, "On the noise reduction mechanisms of porous aerofoil leading edges," Journal of Sound and Vibration (2020) doi: j.jsv.2020.115574.

[34]C. Ocker, F. Czwielong, T. F. Geyer, P. Chaitanya, M. Merkel, and S. Becker, "Permeable structures for leading edge noise reduction," AIAA AVIATION 2021 FORUM, AIAA-2021-2192 (2021).

[35]C. Ocker, T. F. Geyer, F. Czwielong, F. Krömer, W. Pannert, M. Merkel, and S. Becker, "Permeable Leading Edges for Airfoil and Fan Noise Reduction in Disturbed Inflow," AIAA Journal **59**(12), 4969–4986 (2021) doi: 10.2514/1.J060396.

[36]Y. D. Mayer, H. K. Jawahar, M. Szőke, S. A. S. Ali, and M. Azarpeyvand, "Design and performance of an aeroacoustic wind tunnel facility at the university of bristol," Applied Acoustics **155**, 358 – 370 (2019) doi: https://doi.org/10.1016/j.apacoust.2019.06.005.

[37]A. P. G. Sagrado, "Boundary layer and trailing edge noise sources," Ph.D. Thesis, University of Cambridge (2008).

[38]Y. Mayer, B. Zang, and M. Azarpeyvand, "Near-field aeroacoustic characteristics of a stalled naca 0012 aerofoil," in *Proceedings of the 23rd International Congress on Acoustics, integrating 4th EAA Euroregio 2019*, edited by M. Ochmann, Proceedings of the ICA AND EAA EUROREGIO, DEGA e.V. (2019), pp. 5421–5428.

[39]L. Bowen, A. Celik, M. Azarpeyvand, and C. R. I. da Silva, "Grid generated turbulence for aeroacoustic facility," AIAA Journal **60**(3), 1833–1847 (2022) doi: 10.2514/1.J060851.

[40]L. Bowen, A. Celik, M. Azarpeyvand, and C. R. da Silva, "Porous geometry effects on the generation of turbulence interaction noise," in *AIAA AVIATION 2021 FORUM,AIAA 2021-2193*, doi: 10.2514/6.2021-2193.

[41]L. Bowen, A. Celik, M. Azarpeyvand, and C. R. I. da Silva, "On the use of tailored permeable surfaces for turbulence interaction noise control," AIAA AVIATION 2020 FORUM, AIAA-2020-2530 (2020).

[42]L. D. Santana, J. Christophe, C. Schram, and W. Desmet, "A rapid distortion theory modified turbulence spectra for semi-analytical airfoil noise prediction," Journal of Sound and Vibration **383**, 349–363 (2016) doi: https://doi.org/10.1016/j.jsv.2016.07.026.